Inorganic Chemistry

Article

pubs.acs.org/IC

From WCl_6 to WCl_2: Properties of Intermediate Fe–W–Cl Phases

Agnieszka Mos,[†] Cristina Castro,[†,‡] Sylvio Indris,[§] Markus Ströbele,[†] Reinhold F. Fink,[‡] and Hans-Jürgen Meyer*[,†]

[†]Section for Solid State and Theoretical Inorganic Chemistry, Institute of Inorganic Chemistry, and [‡]Institute for Physical and Theoretical Chemistry, University of Tübingen, Auf der Morgenstelle 18, 72076 Tübingen, Germany

[§]Institute for Applied Materials, Karlsruhe Institute of Technology, Post Office Box 3640, 76021 Karlsruhe, Germany

ABSTRACT: Phenomenological studies of WCl_6 reduction with transition metal powders M = Mn, Fe, and Co have been recently reported. These reactions involve a series of reductive intercalation steps of M atoms into layered tungsten chloride arrangements, followed by exsolution of MCl_2. In the series M = Fe, the presence of divalent iron is evidenced for Fe_xWCl_6, FeW_2Cl_{10}, $Fe_2W_2Cl_{10}$, and $(Fe,W)Cl_2$ by Mössbauer spectroscopy. Magnetic properties are reported. Bonding characteristics between tungsten atoms in edge-sharing $[W_2Cl_{10}]^{n-}$ bioctahedra reveal that a double bond can be addressed to FeW_2Cl_{10}. A similar situation appears for $Fe_2W_2Cl_{10}$, due to the localized and thus nonbonding character of the two electrons in the δ orbitals of this compound.

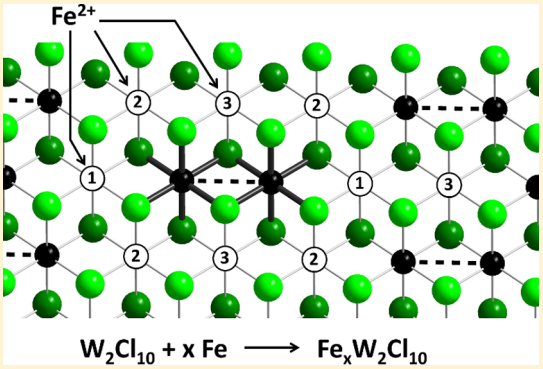

INTRODUCTION

The reduction of tungsten hexachloride has been attempted in many ways, departing from classical[1] and less-common reduction agents. Among the latter, elemental P,[2] Bi,[3] and Fe[4] have been reported as reducing agents for the preparation of W_6Cl_{12}.[5] Recently, intermediate phases such as W_6PCl_{17} and $W_4(PCl)Cl_{10}$,[6] or $(BiCl)[W_6Cl_{14}]$ and $(BiCl_2)[W_6Cl_{13}]$,[7] have been shown to appear in these reductions. Afterward, a more integral approach was introduced for detection and characterization of intermediate phases by combined thermal scanning and structural characterization.

A differential thermal scanning (DTA) approach for the reaction between WCl_6 and iron powder has been explored (Figure 1). This measurement revealed five exothermic effects that can be related to the individual compounds Fe_xWCl_6, FeW_2Cl_{10}, $Fe_2W_2Cl_{10}$, $(Fe,W)Cl_2$, and FeW_6Cl_{14} with increasing temperature.[8] In a following procedure, all intermediate compounds were separately prepared by solid-state reactions. Crystal structures were reported for Fe_xWCl_6,[9] FeW_2Cl_{10}, $Fe_2W_2Cl_{10}$,[8] and FeW_6Cl_{14}[10] on the basis of X-ray powder or single-crystal diffraction techniques. The compound described as $(Fe,W)Cl_2$ has been tentatively addressed with a defect $CdCl_2$-type structure.

After phenomenological studies were performed for reduction of WCl_6 with transition metal powders M = Mn,[11] Fe,[8] and Co,[9] it was clear that not only some structural details but also physical properties and bonding characteristics of these compounds are unknown and raise some interesting questions.

Since these systems have shown behavior closely related to each other with respect to the reaction pathway and their crystal structures, we here present a more detailed analysis of the reduction of tungsten hexachloride with iron powder to make this fundamental study more complete. A model structure is used to explain the reductive intercalation and exsolution of the reducing iron species to visualize the reaction pathway in the lower-temperature regime between 150 and 400 °C. All compounds were prepared by solid-state reactions and treated with solvents in an attempt to remove the $FeCl_2$ side phase, thereby revealing ligand exchange reactions that may open

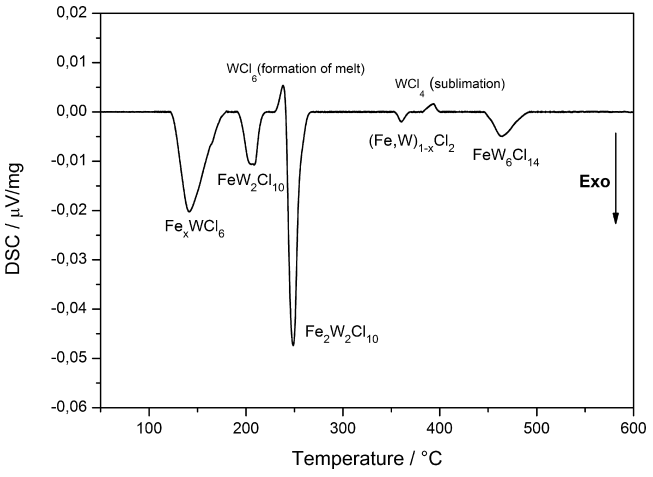

Figure 1. Differential scanning calorimetric (DSC) measurement of a 1:2 molar mixture of WCl_6 and Fe (corrected for background). Endothermic effects near 240 and 400 °C can be attributed to melting of WCl_6 and to sublimation of WCl_4 under given conditions in a fused ampule.

Received: July 15, 2015
Published: October 2, 2015

DOI: 10.1021/acs.inorgchem.5b01574
Inorg. Chem. 2015, 54, 9826–9832

Scheme 1

$$WCl_6 \xrightarrow{+Fe} Fe_xWCl_6 \xrightarrow{+Fe} FeW_2Cl_{10} \xrightarrow{+Fe} Fe_2W_2Cl_{10} \longrightarrow (Fe,W)Cl_2 \xrightarrow{-FeCl_2} FeW_6Cl_{14} \xrightarrow{-FeCl_2} W_6Cl_{12}$$

interesting ways for syntheses of metal organic compounds. Structural and analytical data are collected for FeW_2Cl_{10} and $(Fe,W)Cl_2$. Mössbauer spectroscopy and magnetic measurements are performed to analyze oxidation states and magnetic properties of these compounds. Furthermore, the bioctahedral $[W_2Cl_{10}]^{n-}$ unit is studied by quantum chemical calculations to get more insight into the unexpected similarity of W−W distances in FeW_2Cl_{10} and $Fe_2W_2Cl_{10}$

EXPERIMENTAL SECTION

Samples of Fe_xWCl_6, FeW_2Cl_{10}, $Fe_2W_2Cl_{10}$, $(Fe,W)Cl_2$, and FeW_6Cl_{14} were prepared as previously reported, in an attempt to achieve high-purity samples.[8] Single crystals of FeW_2Cl_{10} were obtained for the first time from a mixture of WCl_6 and Fe powder (total mass ca. 250 mg) reacted for 100 h in a fused silica tube at 270 °C following reaction 1:

$$2WCl_6 + 2Fe \rightarrow FeW_2Cl_{10} + FeCl_2 \quad (1)$$

FeW_2Cl_{10} was treated with different solvents in an attempt to remove $FeCl_2$ side phases. Upon treatment with dry ethanol, single crystals of $W_2Cl_4(OEt)_4(EtOH)_2$ and $W_2Cl_4(OEt)_6$ were obtained while the solvent was allowed to evaporate in air. Crystalline powders and single crystals were investigated by X-ray powder and single-crystal diffraction techniques.

X-ray Diffraction. X-ray powder diffraction (XRD) patterns of crystalline powders were collected with a X-ray powder diffractometer (Stoe STADI-P, Ge monochromator) using Cu Kα1 radiation. A single-crystal measurement was performed on a black crystal of FeW_2Cl_{10} with an X-ray single-crystal diffractometer (Stoe IPDS IIT, Darmstadt, Germany), equipped with (graphite) monochromated Mo Kα radiation (λ = 0.710 73 Å). The intensity data were corrected for Lorentz factors and polarization effects by the IPDS software. Absorption effects were corrected by the X-Red/X-Shape program of the Stoe software. The crystal structure for FeW_2Cl_{10} was refined by a full-matrix least-squares method[12] (CSD-429382), yielding results similar to those previously reported on the basis of powder XRD data. FeW_2Cl_{10} powders treated in ethanol revealed surprisingly easy access to compounds $W_2Cl_4(OEt)_4(EtOH)_2$ and $W_2Cl_4(OEt)_6$, whose structures are already reported.[13]

Mössbauer Spectrocopy. ^{57}Fe Mössbauer spectroscopic measurements were performed in transmission mode at room temperature on a constant-acceleration spectrometer with a ^{57}Co(Rh) source. Isomer shifts are given relative to that of α-Fe at room temperature. Measurements were done for Fe_xWCl_6, FeW_2Cl_{10}, $Fe_2W_2Cl_{10}$, and $(Fe,W)Cl_2$. $FeCl_2$ was used as a reference, appearing with the $CdCl_2$ and CdI_2 structure (high-pressure modification) in approximate 1:2 ratio (estimated from the XRD pattern).

Magnetic Measurements. Crystalline samples of compounds were loaded into gelatin capsules under argon atmosphere (glovebox), and their magnetic susceptibilities were recorded with a superconducting quantum interference device (SQUID) magnetometer (Quantum Design, MPMS) with a magnetic field of 100 Oe, in the temperature range 5 K $\leq T \leq$ 300 K with progressive steps (the higher the temperature, the bigger steps between collected data points). The susceptibility of FeW_6Cl_{14} was fitted following an extended Curie−Weiss law [$\chi = C/(T - \theta) + \chi_0$].

Energy-Dispersive X-ray Spectroscopic Measurements. Energy-dispersive X-ray spectroscopic (EDX) data were collected with a transmission electron microscope Hitachi SU8030 at 25.0 kV, allowing quantitative analysis of $(Fe,W)Cl_2$ and revealing the presence of Fe, W, and Cl and the absence of oxide and other elements. Analyses of a series of crystalline specimens gave the average composition $(Fe_{0.37}W_{0.38})Cl_2$ (FeW_6Cl_{14} was used as a standard). Corresponding measurements were performed for $(M,W)Cl_2$ samples with M = Mn, Co, and Ni.

Quantum Chemical Calculations. The bonding characteristics of $[W_2Cl_{10}]^{2-}$ and $[W_2Cl_{10}]^{4-}$ were investigated by spin-unrestricted density functional theory (DFT) calculations performed with the program Turbomole6.6.[14,15] The crystal structure data of FeW_2Cl_{10} and $Fe_2W_2Cl_{10}$ were used as starting points for geometry optimization of both fragments, and no symmetry constraints were imposed. The DFT calculations were carried out with the B3-LYP[16] functional, the RI[17−19] and MARIJ[20] options as well as the def2-TZVP[21] basis set, the Stuttgart small-core pseudopotential,[22] and the COSMO module,[23−25] which was employed to stabilize anions. Geometry-optimized fragments were also analyzed via numerical vibrational analysis,[26] in order to verify the nature of the stationary points found by means of geometry optimization.

RESULTS AND DISCUSSION

Phase Formation and Crystal Structures. WCl_6 can be reduced with a variety of the more electropositive elements from the periodic table. Until now reducing agents such as P, Sb, Bi, and some transition metals (Mn, Fe, Co) have been explored in reactions with tungsten hexahalides by a combined thermal scanning−XRD methodology. Some reactions in these systems appear quite complex due to a number of intermediate stages, as shown in the DTA measurement for reduction of WCl_6 with iron powder in Figure 1. Interpretation of thermal effects involves five exothermic effects that are related to the successive formation of Fe_xWCl_6, FeW_2Cl_{10}, $Fe_2W_2Cl_{10}$, $(Fe,W)Cl_2$, and FeW_6Cl_{14} with increasing temperature, as has been previously reported.[8]

The reaction between WCl_6 and Fe powder begins with a reductive intercalation of iron into the structure of WCl_6, yielding the phase Fe_xWCl_6 ($0 < x < 0.1$) and continues with the formation of FeW_2Cl_{10} and $Fe_2W_2Cl_{10}$, as shown in Scheme 1. These reduction steps are driven by a progressive incorporation of iron into the layered tungsten chloride structure. A turning point is reached with the compound previously described as $(Fe,W)Cl_2$.

The formation of FeW_6Cl_{14} ($PbMo_6Cl_{14}$-type)[27] with an octahedral metal cluster (M_6X_8-type) involves a major rearrangement of atoms, which is unavoidable due to the exsolution of $FeCl_2$ from the structure. Thereby the layered arrangement, evident in all previous structures, is lost. Decomposition of the octahedral tungsten cluster has been previously reported to yield tungsten metal, following the sequence $W_6Cl_{18} \rightarrow W_6Cl_{12} \rightarrow W + Cl_2$ under inert gas flow.[1b]

All compounds in the Fe−W−Cl series were prepared in fused silica tubes under conditions adapted from the DTA measurement. Fe_xWCl_6 ($0 < x < 0.1$) is sensitive to moist air, and samples are intrinsically contaminated from the excess iron powder used in reactions. Single crystals have been previously obtained by sublimation, and the crystal structure has been characterized as (Fe) intercalated (α-)WCl_6 structure.[9] With increasing Fe content, we expected Fe_xWCl_6 to decompose into WCl_5 (W_2Cl_{10}) and $FeCl_2$. Corresponding behavior was obtained for decomposition of $LiWCl_6$ with formation of WCl_5 and LiCl.[28]

FeW_2Cl_{10} is unstable in air and can be washed with dry acetone under argon atmosphere. The crystal structure has been reported on the basis of powder XRD data refinement [$C2/c$, a = 6.1226(1) Å, b = 16.7943(1) Å, c = 12.3737(1) Å, β = 108.99(1)°, V = 1203.1(8) Å^3][8] and is confirmed in this work

DOI: 10.1021/acs.inorgchem.5b01574
Inorg. Chem. 2015, 54, 9826−9832

by single-crystal data [$C2/c$, a = 6.1209(3) Å, b = 16.7771(7) Å, c = 12.3686(6) Å, β = 109.035(4)°, V = 1200.7(1) Å^3].

FeW_2Cl_{10} reacts with ethanol to form deep green single crystals of $W_2Cl_4(OEt)_4(EtOH)_2$[29] and deep red single crystals of $W_2Cl_4(OEt)_6$, shown in Figure 2.[30] Bioctahedral $[W_2Cl_4L_6]$

Figure 2. Green crystals of $W_2Cl_4(OEt)_4(EtOH)_2$ and red crystals of $W_2Cl_4(OEt)_6$ from reactions of FeW_2Cl_{10} in ethanol.

units in both structures contain four terminal chloride ligands. W−W distances were reported in accord to a formal double bond for the W^{4+} species with d_{W-W} = 2.483 Å, and a formal single bond for the W^{5+} species with d_{W-W} = 2.715 Å. The bond lengths and bonding conditions in these compounds appear different than the (μ_2-)chloride-bridged $[W_2Cl_{10}]^{n-}$ bioctahedra in compounds being reported herein.

$Fe_2W_2Cl_{10}$ crystallizes in the same space group $C2/c$ as FeW_2Cl_{10} with a = 6.2486(4) Å, b = 16.734(1) Å, c = 12.637(1) Å, β = 109.713(4)°, and V = 1244.0(2) Å^3. The transition from FeW_2Cl_{10} to $Fe_2W_2Cl_{10}$ requires occupation of just one more octahedral site in the structure with an iron ion, thereby introducing a slight but significant shortening of the W−W distance in the $[W_2Cl_{10}]^{n-}$ bioctahedra from d_{W-W} = 2.707(5) Å (on the basis of powder XRD) or 2.7024(7) Å (single-crystal data) in FeW_2Cl_{10} to d_{W-W} = 2.637(1) Å in $Fe_2W_2Cl_{10}$ (on the basis of powder XRD). Quantum chemical calculations are employed to explore whether this shortening can be considered to represent a transition from W^{4+} to W^{3+}.

Crystal structures of FeW_2Cl_{10} and $Fe_2W_2Cl_{10}$ can be derived from close-packed layers of chloride ions in which iron and tungsten ions occupy 3 of 5 (in FeW_2Cl_{10}) and 4 of 5 (in $Fe_2W_2Cl_{10}$) octahedral voids in every second interlayer. The occupation of another fifth of sites would result in full occupation of all (5 of 5) octahedral sites in every other interlayer, corresponding to the theoretical composition $Fe_3W_2Cl_{10}$ which would require a W^{2+} ion.

The compound originally described as $(Fe,W)Cl_2$ was assigned a defect $FeCl_2$ ($CdCl_2$-type) structure. Carefully recorded powder XRD patterns support the assumption of a defect $CdCl_2$-type structure. XRD studies of $(Fe,W)Cl_2$ samples prepared under different conditions (with respect to reaction time and excess iron powder) have revealed small but significantly deviating lattice parameters indicating a phase width. The observation of some extra reflections in the powder XRD pattern suggests the presence of a superstructure. EDX measurements revealed the composition $(Fe_{0.37}W_{0.38})Cl_2$, which is close to $Fe_2W_2Cl_{10}$. Hence, a cation deficiency is clearly indicated with respect to a $CdCl_2$-type structure. If iron was in divalent and tungsten in trivalent oxidation state, the corresponding charge-balanced phase would be best described as $Fe_{1-x}W_{2/3x}Cl_2$. The presence of a cation deficiency is also supported by other $(M,W)Cl_2$ systems analyzed as $(Mn_{0.47}W_{0.36})Cl_2$,[11] $(Co_{0.24}W_{0.43})Cl_2$,[9] and $(Ni_{0.21}W_{0.54})Cl_2$ by EDX measurements. As long as the precise phase compositions of these compounds remain unknown, we will use the formula $(M,W)_{1-x}Cl_2$.

Crystal structures of FeW_2Cl_{10}, $Fe_2W_2Cl_{10}$, and $(Fe,W)_{1-x}Cl_2$ can be envisioned as an arrangement of close-packed layers of chloride ions, emphasized in Figure 3, and occupied octahedral

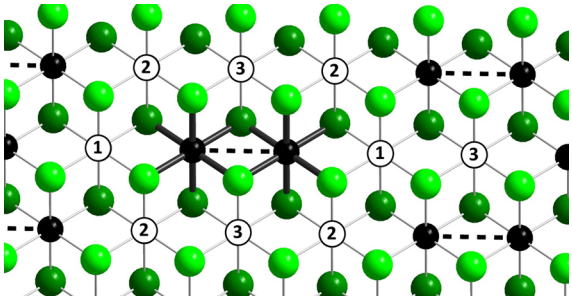

Figure 3. Section of one close-packed double layer made up of chloride ions (light green in front, dark green in back) with 2 of 5 octahedral sites occupied with tungsten ions (black) forming $[W_2Cl_{10}]^{2n-}$ bioctahedra. More octahedral sites are occupied with iron ions, indicated with numbers for FeW_2Cl_{10} (1) and $Fe_2W_2Cl_{10}$ (1 and 2). For $(Fe,W)_{1-x}Cl_2$ (or $Fe_{1-x}W_{2/3x}Cl_2$) we assume a variable (phase-width) cation distribution pattern over all kinds of octahedral sites.

sites in between. Pairs of tungsten ions are embedded into this chloride arrangement to form edge-sharing $[W_2Cl_{10}]^{n-}$ bioctadedra. Displacements of tungsten atom pairs from their octahedral centers toward each other, appearing in real structures, are emphasized only by their connectivity (by a dashed line in the figure). This structural arrangement can be well compared with that of WCl_5, whose arrangement is represented by a bioctahedral $[W_2Cl_{10}]$ unit.[31] Vacant octahedral sites are numbered 1, 2, and 3. Occupation of position 1 with Fe^{2+} corresponds to the crystal structure of FeW_2Cl_{10}, and occupation of positions 1 and 2 represents the structure of $Fe_2W_2Cl_{10}$. An unknown distribution of cations on these sites may be regarded to represent the structure of $(Fe,W)_{1-x}Cl_2$. Alternatively, and in accordance with the general observation that increasing cluster nucleation is obtained with increasing temperature, formation of a higher cluster aggregate such as a trigonal $[W_3Cl_{13}]^{3-}$ cluster would be likely in this system.[32]

Mössbauer Spectroscopy. ^{57}Fe Mössbauer spectra of different samples and their corresponding fitting parameters are displayed in Figure 4 for Fe_xWCl_6, FeW_2Cl_{10}, $Fe_2W_2Cl_{10}$, and $(Fe,W)Cl_2$. A mixture of $CdCl_2$-type[33] and CdI_2-type[34] $FeCl_2$ is used as a reference.

DOI: 10.1021/acs.inorgchem.5b01574
Inorg. Chem. 2015, 54, 9826−9832

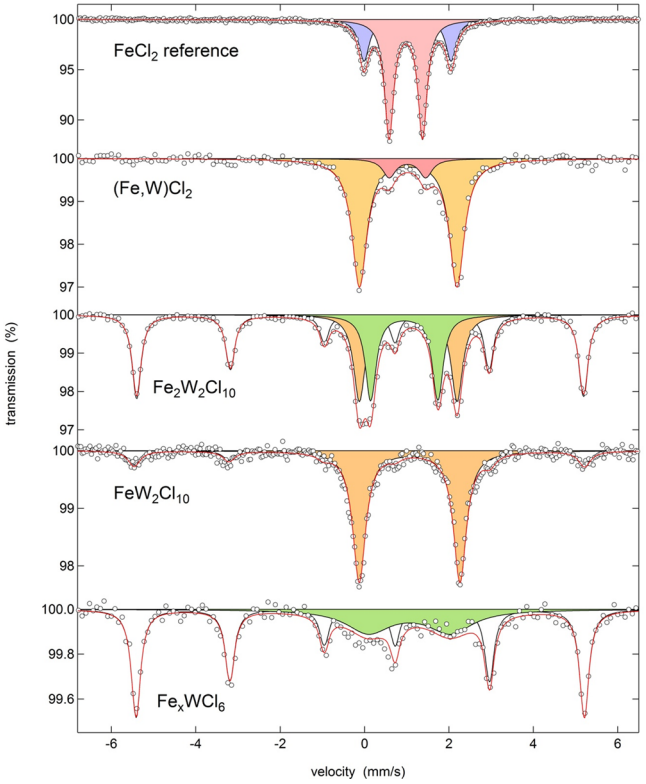

Figure 4. ^{57}Fe Mössbauer spectra including fit (red line). The $FeCl_2$ reference is represented by a mixture of $CdCl_2$ (red fit) and a CdI_2 structured phase (blue fit). Fe^{2+} species present in ternary Fe−W−Cl compounds is fitted (yellow and green). The presence of the iron impurity is represented by characteristic sextet splitting, detectable in spectra of $Fe_2W_2Cl_{10}$, FeW_2Cl_{10}, and Fe_xWCl_6.

The recorded spectra consist of multiple contributions in each case. The presence of metallic Fe shown by the black line with its characteristic (sextet) splitting and position is evident for samples Fe_xWCl_6, FeW_2Cl_{10}, and $Fe_2W_2Cl_{10}$ as a result of the syntheses in which iron powder was employed. Since the value of the density of elemental Fe is high in metallic iron in comparison to the chloride phases, this sextet appears to be very pronounced (see area percentage in Table 1), but the mass fraction of metallic Fe is correspondingly smaller. The other contributions in the spectra are represented exclusively by doublets with isomer shifts in the range from 1.0 to 1.2 mm/s, which is characteristic of Fe^{2+} in high-spin state.[35] Therefore, the presence of Fe^{3+} can be excluded for all samples. The presence of multiple Fe^{2+} doublets reveals different Fe environments, either in the same crystal structure or in different phases.

The disordered situation of Fe^{2+} ions in the structure of Fe_xWCl_6, as refined from a previous single-crystal study, corresponds with a broad doublet. FeW_2Cl_{10} contains one and $Fe_2W_2Cl_{10}$ contains two major doublets, which appear in line with the number of crystallographically distinct Fe^{2+} ions in the respective structures, as also represented by the occupation of positions 1 and 2 in Figure 3. The Mössbauer spectrum of $(Fe,W)Cl_2$ shows essentially one (yellow) doublet and a much smaller (red) one. The smaller (red) one can be addressed as a $FeCl_2$ side phase, indicated by comparison with the (red) $FeCl_2$ reference ($CdCl_2$-type). The presence of just one doublet suggests the presence of only one Fe^{2+} species in the structure of $(Fe,W)Cl_2$. Not unexpectedly, the Mössbauer pattern, and thus the environment of this iron ion, appears similar to that of iron ions in FeW_2Cl_{10} and $Fe_2W_2Cl_{10}$. As can be seen in the Mössbauer spectrum of $Fe_2W_2Cl_{10}$ considerable amount of Fe powder is contained, due to the excess of iron powder used in the reaction. This issue appears to be a problem for the magnetic measurement of this compound.

Magnetic Properties. The magnetic properties of $FeCl_2$ deserve special precaution because $FeCl_2$ is obtained as a side phase in essentially all reactions. Moreover, the crystal structure of $FeCl_2$ ($CdCl_2$-type) is closely related to the layered structures described herein. The magnetic structure of $FeCl_2$ is composed of hexagonal closest-packed layers of ferromagnetically aligned Fe^{2+} spins with a strong anisotropy confining the spins parallel to the hexagonal axis. Alternating layers in this structure are coupled weakly antiferromagnetically to each other, so that the overall magnetic structure is antiferromagnetic below T_N = 23.55 K.[36]

Magnetic susceptibility measurements performed for FeW_2Cl_{10}, $(Fe,W)_{1-x}Cl_2$, and FeW_6Cl_{14} are shown in Figure 5. Measurements on WCl_4 and $FeCl_2$ are used as references. The measurement on WCl_4 shows temperature-independent paramagnetic (TIP) behavior consistent with the consideration

Table 1. Isomer Shifts, Quadrupole Splittings, Hyperfine Fields, and Line Widths Used To Fit Mössbauer Spectra

	IS (mm/s)	QS (mm/s)	B_{hf} (T)	line width (mm/s)	area (%)
		$FeCl_2$			
Fe^{2+}	1.085 ± 0.001	0.790 ± 0.001		0.263 ± 0.001	68.5
Fe^{2+}	1.125 ± 0.001	2.062 ± 0.003		0.299 ± 0.004	31.5
		$(Fe,W)Cl_2$			
Fe^{2+}	1.141 ± 0.002	2.310 ± 0.005		0.427 ± 0.008	88.8
Fe^{2+}	1.124 ± 0.016	0.865 ± 0.031		0.373 ± 0.048	11.2
		$Fe_2W_2Cl_{10}$			
Fe^{2+}	1.141 ± 0.005	2.315 ± 0.006		0.330 ± 0.009	30.8
Fe^{2+}	1.048 ± 0.003	1.589 ± 0.007		0.307 ± 0.010	26.4
Fe^{0}	−0.005 ± 0.002	0.009 ± 0.004	32.8 ± 0.1	0.255 ± 0.007	42.8
		FeW_2Cl_{10}			
Fe^{2+}	1.174 ± 0.002	2.388 ± 0.004		0.374 ± 0.006	81.8
Fe^{0}	−0.016 ± 0.013	0.001 ± 0.027	33.1 ± 0.1	0.349 ± 0.040	18.2
		Fe_xWCl_6			
Fe^{2+}	1.172 ± 0.036	1.950 ± 0.062		1.274 ± 0.101	35.7
Fe^{0}	−0.004 ± 0.003	0.011 ± 0.006	32.9 ± 0.1	0.263 ± 0.008	64.2

DOI: 10.1021/acs.inorgchem.5b01574
Inorg. Chem. 2015, 54, 9826−9832

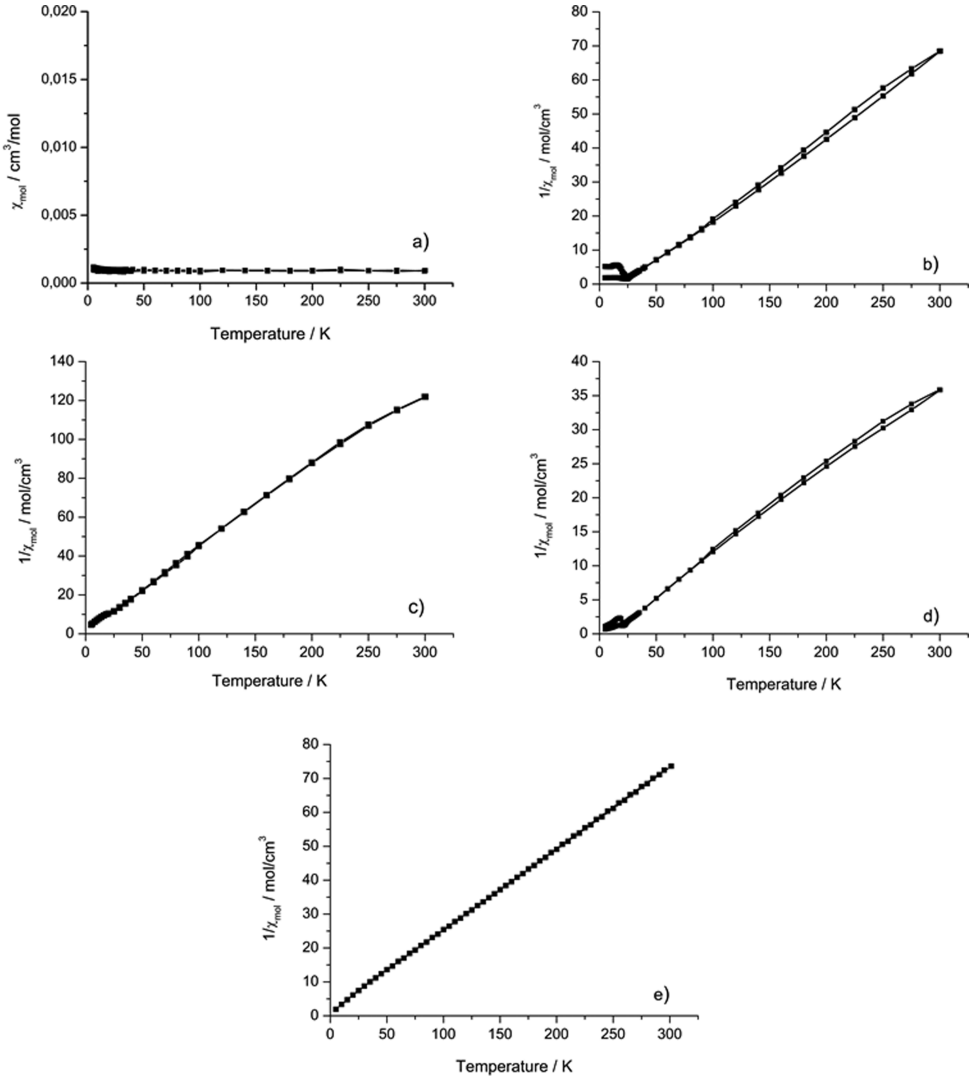

Figure 5. Temperature dependency of magnetic susceptibilities of (a) WCl_4, (b) $FeCl_2$, (c) $(Fe,W)_{1-x}Cl_2$, (d) FeW_2Cl_{10}, and (e) FeW_6Cl_{14} measured in field-cooled (FC) and zero-field-cooled (ZFC) modes.

of W^{4+} ions and electrons being semilocalized in formally double-bonded W−W dumbbells. In comparison, the formula FeW_2Cl_{10} can be decomposed into $FeCl_2$ and two times WCl_4, yielding four unpaired electrons from one (high-spin d^6) Fe^{2+} ion per formula unit, responsible for paramagnetic behavior. Antiferromagnetic ordering obtained in the plots of FeW_2Cl_{10} and $(Fe,W)_{1-x}Cl_2$ at 24 K can be attributed to the presence of the $FeCl_2$ side phase.

Paramagnetic behavior is found for FeW_6Cl_{14}. The fit with an extended Curie−Weiss law corresponds to the expected value of 5.3μ_B, consistent with one Fe^{2+} and a diamagnetic $[W_6Cl_{14}]^{2-}$ cluster.

Electronic Structure. The crystal structures of FeW_2Cl_{10} and $Fe_2W_2Cl_{10}$ contain edge-sharing $[W_2Cl_{10}]^{n-}$ bioctahedra, which can be derived from the structure of tungsten pentachloride. The crystal structure of WCl_5 contains two independent but only slightly distinct W_2Cl_{10} molecules, having W−W distances of 3.816(2) and 3.813(1) Å.[31]

The short W−W bond distance is of particular interest for these substances. Thus, we investigated it by quantum chemical approaches with $[W_2Cl_{10}]^{n-}$ clusters as model systems. Hereby we assume that the electronic structure, and in particular the bond distances, are only marginally influenced by the surrounding clusters. This assumption is motivated by the much longer bond distances for Fe−W (3.59−3.72 Å), Fe−Fe (3.71 Å), and Fe−Cl (2.28−2.64 Å) as compared to W−W (2.64/2.70 Å) and W−Cl (2.29−2.49 Å). Bonding and antibonding interactions between the three t_{2g} d-orbitals in the bioctahedral $[W_2Cl_{10}]^{n-}$ ion are expected to lead to a molecular orbital (MO) scheme following the order $\sigma < \pi < \delta < \delta^* < \pi^* < \sigma^*$ levels with increasing energy (Figure 6). The occupation of these levels from d^1−d^1 to d^6−d^6 configurations involve various electronic situations in which the d^6−d^6 configuration would represent the absence of metal−metal bonding.[37,38]

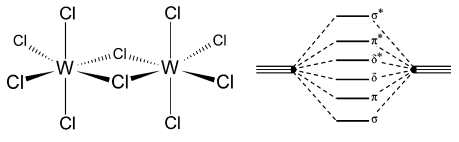

Figure 6. Structure of a bioctahedral $[W_2Cl_{10}]^{n-}$ fragment (left) and energy splitting of t_{2g}-type levels for occupation of bonding and antibonding W−W states (right).

DOI: 10.1021/acs.inorgchem.5b01574
Inorg. Chem. 2015, 54, 9826−9832

A deviation from the above-mentioned energy level order has to be considered in the present case. Calculations find that the δ level is destabilized through interactions with (μ_2)-bridging halides (orbitals) of the same symmetry (Figure 7).[39−44]

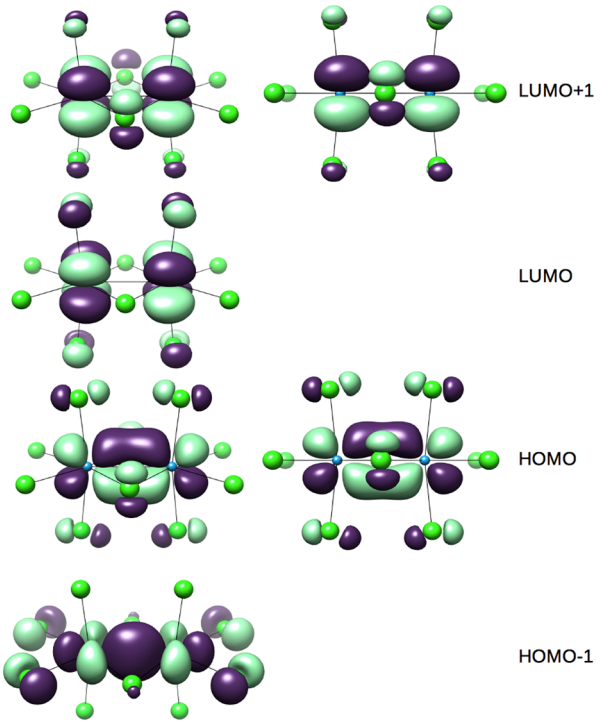

Figure 7. Molecular orbitals of the $[W_2Cl_{10}]^{2-}$ anion representing σ (HOMO − 1) and π (HOMO) molecular orbitals, as well as the energy inversion of δ (LUMO) and δ^* (LUMO + 1) levels as a result of the particular linear combination of d-type orbitals with p orbitals of bridging chloride ions. Orbitals at right are rotated to highlight the π-type bonding (below) and the antibonding situation between δ-type molecular orbitals and p orbitals of bridging chloride ions. All molecular orbitals have been rendered[51] with an isovalue of 0.045. HOMO, highest occupied molecular orbital; LUMO, lowest unoccupied molecular orbital.

Thereby the δ level is moved slightly above the δ^* level. The electronic configuration of the ground state has been assigned as $\sigma^2\pi^2\delta^{*2}$ by an analysis of the apparent metal−metal distance.[45] However, calculations and the near-degeneracy of δ and δ^* orbitals support antiferromagnetic ordering within bioctahedral tungsten clusters for d^3−d^3 situations with a ground state composed of about 50% each $\sigma^2\pi^2\delta^{*2}$ and $\sigma^2\pi^2\delta^2$ configurations. This is equivalent to the occupation pattern $\sigma^2\pi^2\delta^{*1}\delta^1$ for $Fe_2W_2Cl_{10}$. According to McGrady et al.,[42] the inversion of the δ and δ^* levels is lifted only if the metal−metal distance becomes shorter than 2.3 Å. In this case a W−W triple bond and a sequence of energy levels corresponding to the molecular orbitals shown in Figure 6 is expected.

FeW_2Cl_{10} contains the $[W_2Cl_{10}]^{2-}$ ion, which can be related to the diamagnetic WCl_4 with a d^2−d^2 interaction formally consistent with a ($\sigma^2\pi^2$) double bond. W−W distances, d_{W-W} = 2.707(5) Å for FeW_2Cl_{10}, are in line with our calculated value (d_{W-W} = 2.719 Å) as well as crystal structure values reported for WCl_4 [d_{W-W} = 2.688(2) Å[46] or 2.713(3) Å[47]], and $(NR_4)_2(W_2Cl_{10})$ [d_{W-W} = 2.792(1) Å].[48] The results of our calculations on bioctahedral $[W_2Cl_{10}]^{2-}$ ions are represented by the molecular orbitals shown in Figure 7. The HOMO − 1 represents the σ-type bond, and the HOMO represents a π-type bond for the W−W dumbbell of W^{4+} ions in $[W_2Cl_{10}]^{2-}$. For this cluster, but also for the d^3 analogue $[W_2Cl_{10}]^{4-}$ and in line with former quantum chemical results, an inversion of δ/δ^* type levels is found.

The situation of $[W_2Cl_{10}]^{4-}$ in $Fe_2W_2Cl_{10}$ with a d^3−d^3 interaction appears more complicated due to occupation of δ and δ^* levels. The W−W distance, d_{W-W} = 2.637(1) Å in $Fe_2W_2Cl_{10}$, is well reproduced with our calculations, which provide d_{W-W} = 2.644 Å. It is expected that the W(d^3)−W(d^3) bond distance with an effective orbital occupation of $\sigma^2\pi^2\delta^{*1}\delta^1$ is similar to the distance between the W(d^2)−W(d^2) centers with the configuration $\sigma^2\pi^2$, as both cases correspond to a formal double bond. We note that occupation of bonding δ and antibonding δ^* orbitals, with a preference for the occupation of the latter orbital in $[W_2Cl_{10}]^{4-}$, is expected to lead to weaker bonding than in $[W_2Cl_{10}]^{2-}$. Thus, this effect should be small as δ bonding and antibonding is relatively weak.

We considered two possible explanations for the increased bond strength of the W(d^3)−W(d^3) cluster as compared with the W(d^2)−W(d^2) one: first, occupation of the δ orbitals increases the number of electrons at the tungsten atoms and thus lowers the electronegativity of this center. Thus, the tungsten d-orbitals become more diffuse, which leads to a stronger σ- and π-bonding. This argument is supported by the Mayer bond order[49] of these complexes, which was found to be 1.39 for $[W_2Cl_{10}]^{2-}$ and 1.62 for $[W_2Cl_{10}]^{4-}$. An alternative explanation for the observed bond distance difference is that the effective (positive) charge at the tungsten atoms decreases with reduction of $[W_2Cl_{10}]^{2-}$ to $[W_2Cl_{10}]^{4-}$. Indeed, natural population analysis (NPA)[50] indicates a slightly smaller charge of the W atoms in $[W_2Cl_{10}]^{4-}$ (0.510e) than in $[W_2Cl_{10}]^{2-}$ (0.541e). Thus, smaller Coulomb repulsion between the tungsten centers is another possible explanation for the observed bond distance differences. The small absolute change of NPA charges and the rather significant difference between Mayer bond orders indicate that the latter may be more important for observed bond distance changes.

CONCLUSION

Reduction of WCl_6 with a sufficient amount of iron powder involves the compounds FeW_2Cl_{10}, $Fe_2W_2Cl_{10}$, $(Fe,W)_{1-x}Cl_2$, and FeW_6Cl_{14}. Crystal structures of FeW_2Cl_{10}, and $Fe_2W_2Cl_{10}$ reflect successive steps of reductive intercalations of Fe atoms into a W_2Cl_{10} (WCl_5) structure.[31] This reductive intercalation can be considered to require a minimum of energy because no fundamental structural reorganization is necessary.

Mössbauer studies clearly show that iron ions are always present as Fe^{2+}. Following this result, tungsten appears as W^{4+} in FeW_2Cl_{10} and as W^{3+} in $Fe_2W_2Cl_{10}$ and probably also in $(Fe,W)_{1-x}Cl_2$. The bonding between tungsten ions in edge-sharing $[W_2Cl_{10}]^{n-}$ bioctahedra can be characterized as a W^{4+}−W^{4+} interaction with a formal ($\sigma^2\pi^2$) double bond for FeW_2Cl_{10}. The situation of W^{3+}−W^{3+} interaction in $Fe_2W_2Cl_{10}$ can be also assigned close to a double bond because the delta orbitals are nearly nonbonding, due to the equal occupation of δ and δ^* levels with one electron.

AUTHOR INFORMATION

Corresponding Author

*E-mail: Juergen.meyer@uni-tuebingen.de.

DOI: 10.1021/acs.inorgchem.5b01574
Inorg. Chem. 2015, 54, 9826−9832

Notes

The authors declare no competing financial interest.

■ ACKNOWLEDGMENTS

This research was supported by the Deutsche Forschungsgemeinschaft (Bonn) via Grant ME 914/27-1. We express our gratitude to Dr. Jochen Glaser (Universität Tübingen) for magnetic measurements and for helpful discussions. We also thank Stefan Behnle (Universität Tübingen) for computational assistance. Elke Nadler is gratefully acknowledged for performing the EDX measurements, which have been facilitated by Prof. Dr. Thomas Chassé (Universität Tübingen).

■ REFERENCES

(1) (a) Siepmann, R.; von Schnering, H. G.; Schäfer, H. *Angew. Chem., Int. Ed. Engl.* **1967**, *6*, 637−637. (b) Nägele, A.; Glaser, J.; Meyer, H.-J. *Z. Anorg. Allg. Chem.* **2001**, *627*, 244−249. (c) Dill, S.; Glaser, J.; Ströbele, M.; Tragl, S.; Meyer, H.-J. *Z. Anorg. Allg. Chem.* **2004**, *630*, 987−992.
(2) (a) Novikov, G. I.; Andreeva, N. V.; Polyachenok, O. G. *Russ. J. Inorg. Chem.* **1961**, *6*, 1990−1993. (b) Kolesnichenko, V.; Swenson, D.; Messerle, L. *Inorg. Chem.* **1998**, *37*, 3257−3262.
(3) (a) Kolesnichenko, V.; Messerle, L. *Inorg. Chem.* **1998**, *37*, 3660−3663. (b) Ströbele, M.; Jüstel, T.; Bettentrup, H.; Meyer, H.-J. *Z. Anorg. Allg. Chem.* **2009**, *635*, 822−827. (c) Ströbele, M.; Meyer, H.-J. *Z. Anorg. Allg. Chem.* **2009**, *635*, 1517−1519.
(4) Zhang, X.; McCarley, R. E. *Inorg. Chem.* **1995**, *34*, 2678−2683.
(5) von Schnering, H. G.; May, W.; Peters, K. *Z. Kristallogr.* **1993**, *208*, 368−369.
(6) Ströbele, M.; Meyer, H.-J. *Z. Anorg. Allg. Chem.* **2009**, *635*, 1517−1519.
(7) Ströbele, M.; Eichele, K.; Meyer, H.-J. *Eur. J. Inorg. Chem.* **2011**, *2011*, 4063−4068.
(8) Ströbele, M.; Mos, A.; Meyer, H.-J. *Inorg. Chem.* **2013**, *52*, 6951−6956.
(9) Mos, A.; Ströbele, M.; Meyer, H.-J. *J. Cluster Sci.* **2015**, *26*, 187−198.
(10) Ströbele, M.; Meyer, H.-J. *Z. Anorg. Allg. Chem.* **2011**, *637*, 1024−1029.
(11) Mos, A.; Ströbele, M.; Meyer, H.-J. *Z. Anorg. Allg. Chem.* **2015**, *641*, 1722−1727.
(12) Sheldrick, G. M. *Acta Crystallogr., Sect. A: Found. Crystallogr.* **2008**, *64*, 112−122.
(13) Cotton, F. A.; Falvello, L. R.; Fredrich, M. F.; DeMarco, D.; Walton, R. A. *J. Am. Chem. Soc.* **1983**, *105*, 3088−3097.
(14) *Turbomole*, v6.6, 2014, a development of the University of Karlsruhe and Forschungszentrum Karlsruhe GmbH, 1989−2007; Turbomole GmbH, since 2007; available from www.turbomole.com.
(15) Ahlrichs, R.; Bär, M.; Häser, M.; Horn, H.; Kölmel, C. *Chem. Phys. Lett.* **1989**, *162*, 165−169.
(16) Becke, A. D. *Phys. Rev. A: At., Mol., Opt. Phys.* **1988**, *38*, 3098−3100.
(17) Vahtras, O.; Almlöf, J.; Feyereisen, M. W. *Chem. Phys. Lett.* **1993**, *213*, 514−518.
(18) Eichkorn, K.; Weigend, F.; Treutler, O.; Ahlrichs, R. *Theor. Chem. Acc.* **1997**, *97*, 119−124.
(19) von Arnim, M.; Ahlrichs, R. *J. Comput. Chem.* **1998**, *19*, 1746−1757.
(20) Sierka, M.; Hogekamp, A.; Ahlrichs, R. *J. Chem. Phys.* **2003**, *118*, 9136−9148.
(21) Weigend, F.; Ahlrichs, R. *Phys. Chem. Chem. Phys.* **2005**, *7*, 3297−3305.
(22) Andrae, D.; Häußermann, U.; Dolg, M.; Stoll, H.; Preuß, H. *Theor. Chim. Acta* **1990**, *77*, 123−141.
(23) Klamt, A.; Schüürmann, G. *J. Chem. Soc., Perkin Trans. 2* **1993**, *2*, 799−805.
(24) Klamt, A. *J. Phys. Chem.* **1996**, *100*, 3349−3353.
(25) Klamt, A.; Jonas, V. *J. Chem. Phys.* **1996**, *105*, 9972−9981.
(26) Deglmann, P.; Furche, F.; Ahlrichs, R. *Chem. Phys. Lett.* **2002**, *362*, 511−518.
(27) Böschen, S.; Keller, H.-L. *Z. Kristallogr.* **1992**, *200*, 305−315.
(28) Weisser, M.; Tragl, S.; Meyer, H.-J. *Z. Kristallogr. - New Cryst. Struct.* **2007**, *223*, 5−6.
(29) Anderson, L. B.; Cotton, F. A.; DeMarco, D.; Fang, A.; Ilsley, W. H.; Kolthammer, B. W. S.; Walton, R. A. *J. Am. Chem. Soc.* **1981**, *103*, 5078−5086.
(30) Cotton, F. A.; DeMarco, D.; Kolthammer, B. W. S.; Walton, R. A. *Inorg. Chem.* **1981**, *20*, 3048−3051.
(31) Cotton, F. A.; Rice, C. E. *Acta Crystallogr., Sect. B: Struct. Crystallogr. Cryst. Chem.* **1978**, *B34*, 2833−2834.
(32) Weisser, M.; Tragl, S.; Meyer, H.-J. *Z. Anorg. Allg. Chem.* **2006**, *632*, 1885−1889.
(33) Wilkinson, M. K.; Cable, J. W.; Wollan, E. O.; Koehler, W. C. *Phys. Rev.* **1959**, *113*, 497−507.
(34) Vettier, C.; Yelon, W. B. *J. Phys. Chem. Solids* **1975**, *36*, 401−405.
(35) Menil, F. *J. Phys. Chem. Solids* **1985**, *46*, 763−769.
(36) Birgeneau, R. J.; Yelon, W. B.; Cohen, E.; Makovsky, J. *Phys. Rev. B* **1972**, *5*, 2607−2615.
(37) Poli, R.; Torralba, R. C. *Inorg. Chim. Acta* **1993**, *212*, 123−134.
(38) Cotton, F. A.; Dunbar, K. R.; Eagle, C. T.; Falvello, L. R.; Price, A. C. *Inorg. Chem.* **1989**, *28*, 1754−1757.
(39) Stranger, R.; Lovell, T.; McGrady, J. E. *Inorg. Chem.* **1999**, *38*, 5510−5518.
(40) Shaik, S.; Hoffmann, R.; Fisel, C. R.; Summerville, R. H. *J. Am. Chem. Soc.* **1980**, *102*, 4555−4572.
(41) Brogden, D. W.; Turov, Y.; Nippe, M.; Li Manni, G.; Hillard, E. A.; Clérac, R.; Gagliardi, L.; Berry, J. F. *Inorg. Chem.* **2014**, *53*, 4777−4790.
(42) McGrady, J. E.; Stranger, R.; Lovell, T. *Inorg. Chem.* **1998**, *37*, 3802−3808.
(43) Cavigliasso, G.; Yu, C.-Y.; Stranger, R. *Polyhedron* **2007**, *26*, 2942−2948.
(44) Chiarella, G. M.; Cotton, F. A.; Murillo, C. A.; Zhao, Q. *Inorg. Chem.* **2014**, *53*, 2288−2295.
(45) Canich, J. A. M.; Cotton, F. A.; Daniels, L. M.; Lewis, D. B. *Inorg. Chem.* **1987**, *26*, 4046−4050.
(46) Nägele, A. Dissertation, University of Tübingen, Germany, 2001.
(47) Kolesnichenko, V.; Swenson, D. C.; Messerle, L. *Inorg. Chem.* **1998**, *37*, 3257−3262.
(48) Kolesnichenko, V.; Swenson, D. C.; Messerle, L. *Chem. Commun.* **1998**, 2137−2138.
(49) Mayer, I. *Chem. Phys. Lett.* **1983**, *97*, 270−274.
(50) Reed, A. E.; Weinstock, R. B.; Weinhold, F. *J. Chem. Phys.* **1985**, *83*, 735−746.
(51) Pettersen, E. F.; Goddard, T. D.; Huang, C. C.; Couch, G. S.; Greenblatt, D. M.; Meng, E. C.; Ferrin, T. E. *J. Comput. Chem.* **2004**, *25*, 1605−1612.

DOI: 10.1021/acs.inorgchem.5b01574
Inorg. Chem. 2015, 54, 9826−9832